

Mesoscale and Microscale Observations of Biological Growth in a Silicon Pore Imaging Element

HUBERT J. DUPIN AND
PERRY L. MCCARTY*

Department of Civil and Environmental Engineering,
Stanford University, Stanford, California 94305-4020

Better physical understanding is needed of the processes affecting biological growth in aquifers, filtration beds, and recharge basins. Toward this end, a two-dimensional random width network pore model etched in a silicon wafer was developed to simulate microbial growth in porous media representative of fine sand. This Silicon Pore Imaging Element (SPIE) was seeded with a mixed culture and fed with 0.34 mM acetate under aerobic conditions and at fixed flow rate. Twelve filamentous colonies grew in a dense manner in the upgradient and lateral directions and at low density in the downgradient direction. Heterogeneous colonization led to empty zones. Particle tracking suggested rerouting of flow due to biomass growth. Microscale time-lapse measured filamentous growth rates (0.5 to 1.6 $\mu\text{m}/\text{min}$) were in good agreement with measured mesoscale colony expansion rates. Rather than the microscale concept of biomass developing at the surface of soil grains, filamentous growth may be better represented as mesoscale colonies spanning over several pores and separated from each other by open flow channels. Biological clogging might be prevented if such flow channels could be kept open in some manner.

Introduction

The factors contributing to biological clogging of filtration beds, recharge basins, and aquifers during in-situ bioremediation are yet poorly understood. Investigators have studied biological clogging effects from change in flow rate under constant head conditions (1–3) and biomass build-up (4–6). Clogging is reported to result from liquid porosity reduction due to biofilm growth (1, 4), from the formation of biomass aggregates plugging pore necks (4, 7), from the production of extra-cellular polymers that fill the pores (6), from the formation of gas bubbles that prevent liquid flow (8), and from an increase in pore channel friction factor (9).

Different factors affecting clogging can result because of different circumstances, including the particular microbial strains, nutrients, hydrodynamics (particularly shear), grain size, and applications of interest (sand filtration, wastewater injection, well pumping, bioremediation, enhanced oil recovery). Some authors have addressed specific phenomena such as liquid flow within biofilm (10, 11), colonization (12), attachment (13), profiles of oxygen concentration throughout an aggregate of microorganisms (14), the relationship between substrate concentration, and hydrodynamic boundary layers over biofilm (15). While such studies provide insight

into basic phenomena, the observations are generally limited because of difficulties in directly observing changes in growth patterns with time.

Most observations of biological clogging have been made at the end of an experiment after the porous media are dismantled. In part to overcome these difficulties, Cunningham et al. (1) evaluated growth and clogging using glass beads as the porous media. Because such experimental data is sparse in the literature, biological growth and clogging in porous media is mainly modeled as resulting from growth of a continuous biofilm developing at the surface of grains (16–18) or sometimes resulting from growth of microcolonies (19). However, Vandevivere et al. (20) indicated that by assuming only the presence of a continuous biofilm, permeability reduction may be underestimated significantly.

Thus, there is an additional need for a global understanding of bioclogging that can best be obtained by direct microscopic observations of biological growth in pores over time and space. Directed toward this need, we have developed an apparatus similar to that by Paulsen et al. (21) that permits such observations of biological growth using a two-dimensional micromodel of porous media etched in silicon wafers, which we call a Silicon Pore Imaging Element (SPIE). A description of the apparatus for observing and recording growth in a SPIE is given in the following together with one illustrative example from an experiment using a random network pore structure.

Material and Methods

SPIE Construction and Operation. Two-dimensional physical simulators of porous media etched in glass or silicon have been used over the past decade by petroleum engineers to allow real time microscopic or mesoscopic observations of two- and three-phase flow. Such models can be of a regular (14, 22) or random (21, 23) pattern. Network models can simulate many aspects of heterogeneous porous media (24) and allow numerical simulation of flow patterns. Additionally, progress in semiconductor manufacturing now allows manufacturing of SPIEs of any geometry, with high accuracy (submicronic details) and with good depth of etching (100–200 μm).

The SPIE reported here to evaluate bioclogging of porous media had a geometry consisting of an array of nodes connected by channels (ball-and-stick network model) as illustrated in Figure 1. The full SPIE was 13.5 mm wide and 28 mm long and contained a 28×57 square grid with nodes spaced 0.5 mm apart. The 3107 resulting rectangular channels had widths randomly drawn from the commonly used log-normal distribution, with a mean of 75 μm , a standard deviation of 47 μm , and minimum and maximum values of 50 and 200 μm , respectively. Each node was circular with a diameter equaling the maximum of the widths of the incoming channels; thus, channel lengths were somewhat different. The resulting network was isotropic and homogeneous at the Darcy scale. Because of the grain sizes (about 0.5 mm), the pore sizes (50–200 μm), and the skewed distribution of pore sizes, the SPIE simulated pore spaces in a fine homogeneous sand. The resulting volume of the voids was 28 mm^3 based on an etching depth of 200 μm . The porosity was 37%.

Wafer Etching. The SPIEs were produced at the Stanford Nanofabrication Facility. The manufacturing procedure used is summarized below; the full procedures followed up to the etching step are available at <http://www-snf.stanford.edu>.

First several patterns were selected to simulate the porous media geometry of interest. They were computer digitized

* Corresponding author phone: (650)723-4131; fax: (650)725-9474; e-mail: mccarty@cee.stanford.edu.

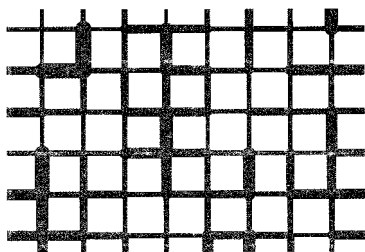


FIGURE 1. Ball and stick network model used for construction of the SPIE used in this experiment. Illustrated is a 4.34 mm \times 3.28 mm section of the SPIE.

and transferred onto a 13 cm chromium mask. Photoresist was deposited in a 7 μ m thick layer on a silicon wafer (type P/Boron, crystal orientation 100, resistivity 20 ohm-cm, 10 cm diameter, 1 mm thick, double-side polished to a 5 μ m total thickness variation (TTV)). A wafer covered by the mask was exposed to UV light, and the portion of the photoresist exposed to UV light was dissolved during development. The wafer was then etched in a plasma at a rate of a few μ m/min, using precautions to keep the trench walls vertical.

After etching to a minimum 210 μ m depth, the photoresist was removed with acetone, and the wafers were cleaned and oxidized in a 80/20 volumetric mixture of sulfuric acid and 30% hydrogen peroxide at 120 $^{\circ}$ C for 20 min. Pyrex wafers (Corning 7740, 10 cm diameter, 0.75 mm thick, double side polished to 10 μ m TTV), used to cover the silicon wafers, were cleaned similarly.

The Pyrex and silicon wafers were rinsed under a stream of water with ultrasound and then spin-dried, using great care to avoid deposition of dust particles. The two wafers were brought into contact (etched side), heated to 350 $^{\circ}$ C, put under a 2×10^{-5} Tor vacuum, and pressed together at 120 N, and 1200 V were applied for 20 min. Anodic bonding was assumed completed when the current stabilized to around 1 mA. The unetched side of the silicon wafer was removed by polishing to expose the etched channels, leaving 200 μ m deep channels with a nominal 10 μ m TTV.

The 10 cm wafers were cut into individual SPIEs, six of which could be prepared on a single silicon wafer. The SPIEs were then exposed to a 25% potassium hydroxide solution at 65 $^{\circ}$ C for 5 min to dissolve residues from processing and then again exposed to the sulfuric acid-hydrogen peroxide mixture to oxidize the surface.

Assembly. A SS 304 stainless steel frame held the SPIE (Figure 2). An upgradient pocket and a downgradient pocket for disinfection were machined in the frame (Figure 3) and conducted water to the SPIE. A UV filter (Shott GG 395, 2 ± 0.05 mm thick, polished to S/D 60-40) was placed over the SPIE. To seal and protect the SPIE, while allowing exposure of the upgradient and downgradient disinfection pockets to UV light, a 2 mm thick Quartz plate (GE 124, transparent to 254 nm UV light) capped the SPIE frame. Water seals, consisting of paraffin film and Viton O-rings, made the SPIE water tight up to 3 m of water head.

A UV lamp (254 nm lamp, model UVG-11, UVP, Upland, CA 91786) was placed 25 cm away from the SPIE during the feeding and at a distance of 3 cm during inoculation to prevent biological growth in the feed and effluent lines.

Image Analysis. *Acquiring.* The SPIE holder was fastened on the traveling stage of a Nikon Diaphot TMD inverted microscope. Two step-motors were fixed on the stage to allow automated movement, each motion step resulting in 3.2 μ m travel on each axis. Resolution was one step in each axis, and repeatability was less than two steps. The motors were PC-controlled through an Anaheim Automation CLCI502 dual axis indexer board. Two TM300 Anaheim Automation step

motor drivers served as a relay between the power supply, the PC board, and the motors.

Observations were made using bright field microscopy. We used a Nikon objective (magnification $\times 10$ /numerical aperture 0.25) and a Nikon lens for the camera (magnification $\times 1$ /field of view number 16). The plane of focus was set to be at middepth of the SPIE and did not offset from this through numerous scans. A Costar CV 252-E CDD camera was used for image acquisition, and an Imagination PX 500 frame grabber was used to transfer the images to a computer. Optimas software was used to analyze the images and communicate with the motor control board. The field of view so obtained was 685 \times 480 μ m, with each pixel representing 1.07 μ m \times 1 μ m. Spatial calibration was obtained by moving the stage a known number of steps several times in each direction and observing the displacement of known features on the screen.

For one complete scan of the SPIE, 1568 stops were programmed. At each stop, eight images were acquired and then averaged to reduce noise before storing. With about 3 s required per saved image, each complete scan of the SPIE required about 1.5 h, and a separate complete scan was acquired every 4–6 h. Once a complete scan was obtained, individual stops could be viewed, or the collection of images representing a complete scan could be concatenated into a meso-image. For the later, each view was shrunk for example to a pixel size of 10 μ m by 10 μ m and placed at its proper position within the overall SPIE to provide the meso-image.

Filtering. Different filters were applied to the concatenated image to enhance viewing of microbial growth. First, a Sobel filter (high pass) was applied, which highlights edges using the square root of the sum of the squares of the gradient in the X and Y directions, using two 3×3 pixels convolution. A dilate filter was used to replace each pixel by the maximum of itself and its eight neighbors, and an erode filter based upon a cross shaped 7×7 pixels kernel was used to remove the edges of the "soil grains" that had been widened by the dilate filter. The resulting image was inverted so that the background was white and the signal (microorganisms) was black. The last filtering process showed overall biological growth on a single meso-image of the entire SPIE.

Growth Measurements. Microorganism growth was observed using rapid time-lapse measurements at two colony leading edge locations (see below). For the first one, images were acquired every minute for 1 h and for the second one, every 30 s for 2 h. Filamentous growth rate was determined by tracking the location of the tip of each filament every 5 min from the collection of time-lapse images. The X and Y coordinates of the filament tip were linearly correlated with time, and from this the rate of filament growth was computed. Measurements were discarded if the coefficients of correlation were less than 0.9 for both coordinates. Growth in the vertical dimension was qualitatively inferred from the variation in the observed thickness of a filament but could not be quantified, and such measurements were discarded.

Flow Measurement. Naturally occurring moving particles were observed using the rapid time-lapse observations. No average liquid flow velocity can be imputed from measured particle velocities because fluid velocity varies widely across a channel with laminar flow and because we had no information on the size of those particles, hence their distance from the plane of focus. However, the observations do give information about flow direction. Artificial calibrated particles were not used here as they might be filtered out by the biomass, which could artificially and significantly enhance plugging of the system because of the high particle density that would be required to sample sufficiently all the streamlines.

SPIE Operation. *Sterilization.* Sterilization of the SPIE was obtained by feeding a degassed 10% nitric acid solution

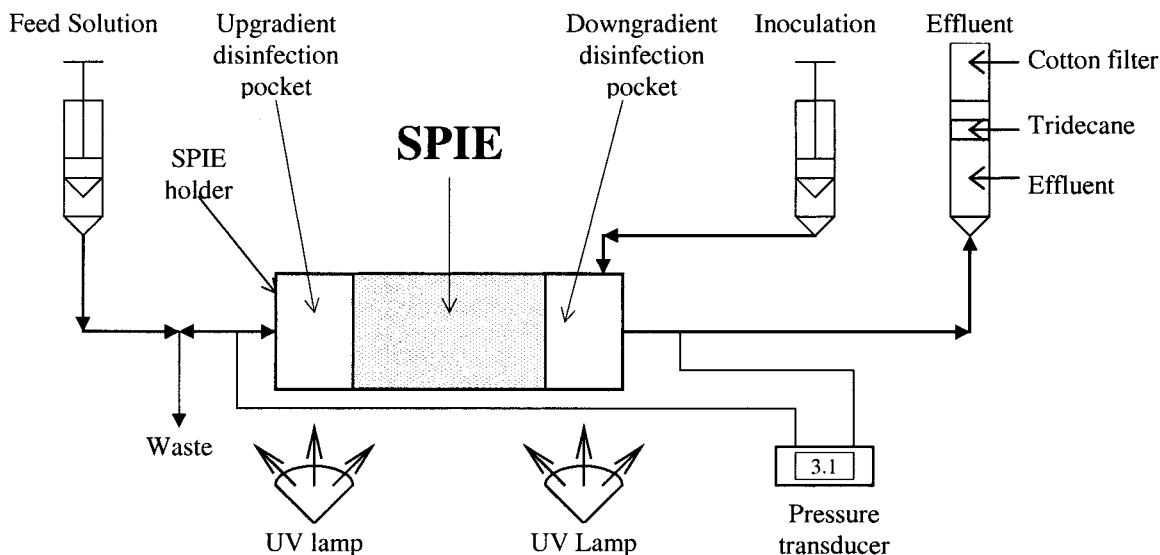


FIGURE 2. Schematic flowchart of the SPIE system. Dead volumes: 1.75 mL from the syringes to the SPIE holder, 0.2 mL from upgradient pocket to waste port valve, 0.028 mL in SPIE porous section, and 0.2 mL each in upgradient and downgradient disinfection pockets. The open-air effluent syringe contained a layer of tridecane to prevent evaporation and was capped by a cotton filter to prevent air-borne contamination.

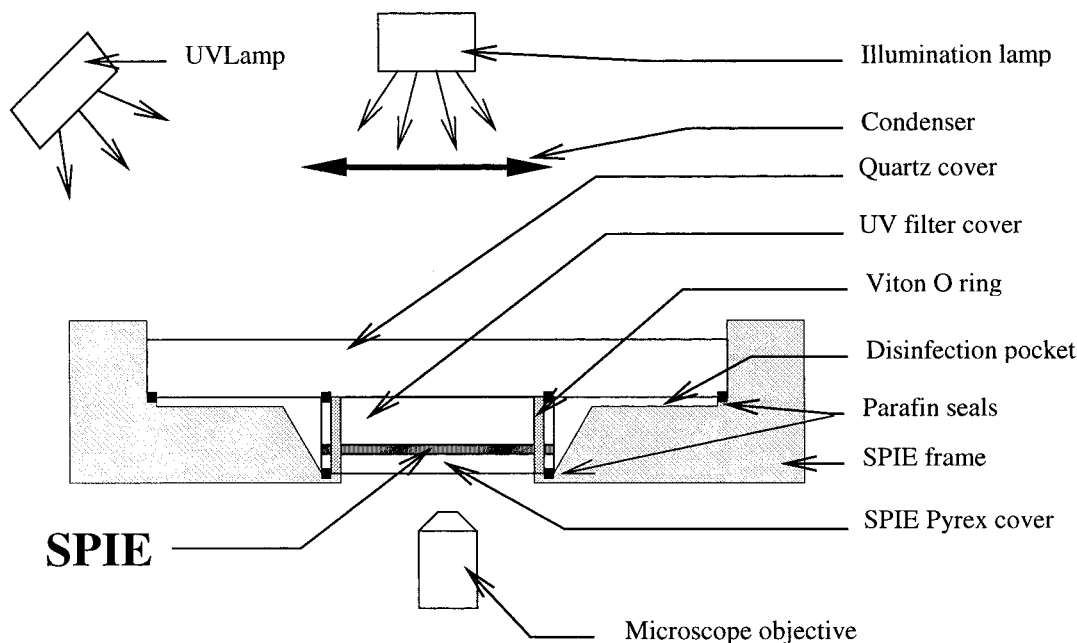


FIGURE 3. Schematic lateral cross-section of the optical setup and SPIE holder

at a rate of 0.2 mL/min for 1 h and rinsing with at least 50 mL of autoclaved demineralized water.

Inoculation. A mixed culture inoculum was prepared using 4 mL of 28-h settled primary effluent from the Palo Alto Water Quality Control Plant added per liter of demineralized water containing 17 mg of KH_2PO_4 , 43.5 mg of K_2HPO_4 , 66.8 mg of $\text{Na}_2\text{HPO}_4 \cdot 7\text{H}_2\text{O}$, 6.8 mg of NH_4Cl , 45 mg of $\text{MgSO}_4 \cdot 7\text{H}_2\text{O}$, 55 mg of CaCl_2 and 0.5 mg of $\text{FeCl}_3 \cdot 6\text{H}_2\text{O}$, to which 1.34 mM $\text{CH}_3\text{COONa} \cdot 3\text{H}_2\text{O}$ (80 mg/L as acetate) was added. The solution was incubated aerobically for 16 h at room temperature while stirring and then diluted 1:10 with demineralized water just before inoculation of the SPIE.

The diluted inoculation solution was fed to the effluent end of the SPIE at 0.1 mL/min for 30 min and then at 0.1 mL/h for 15 min while shining UV light on the influent end at close distance. Inoculation was then stopped, while UV

was shone upgradient and downgradient at close distance for 10 min to prevent growth of microorganisms in the feed and effluent lines. The influent line, which contained sterile demineralized water during inoculation, was then flushed with the following feed solution through the waste line.

Feeding. A feed solution was prepared that contained one-half the mineral concentration of the undiluted incubation solution but only 0.34 mM sodium acetate (20 mg/L as acetate). After autoclaving, the feed solution was vigorously stirred for 30 min at 40 °C while being oxygenated with sterile cotton filtered 99.9% oxygen gas (Liquid Carbonic, Oak Brook, IL 60521). The 40 °C temperature was used to avoid supersaturation and bubble formation in the SPIE.

The feed solution was syringe-pumped into the SPIE influent end at 0.1 mL/h. The effluent was collected in a syringe. The resulting specific discharge rate was 0.89 m/day,

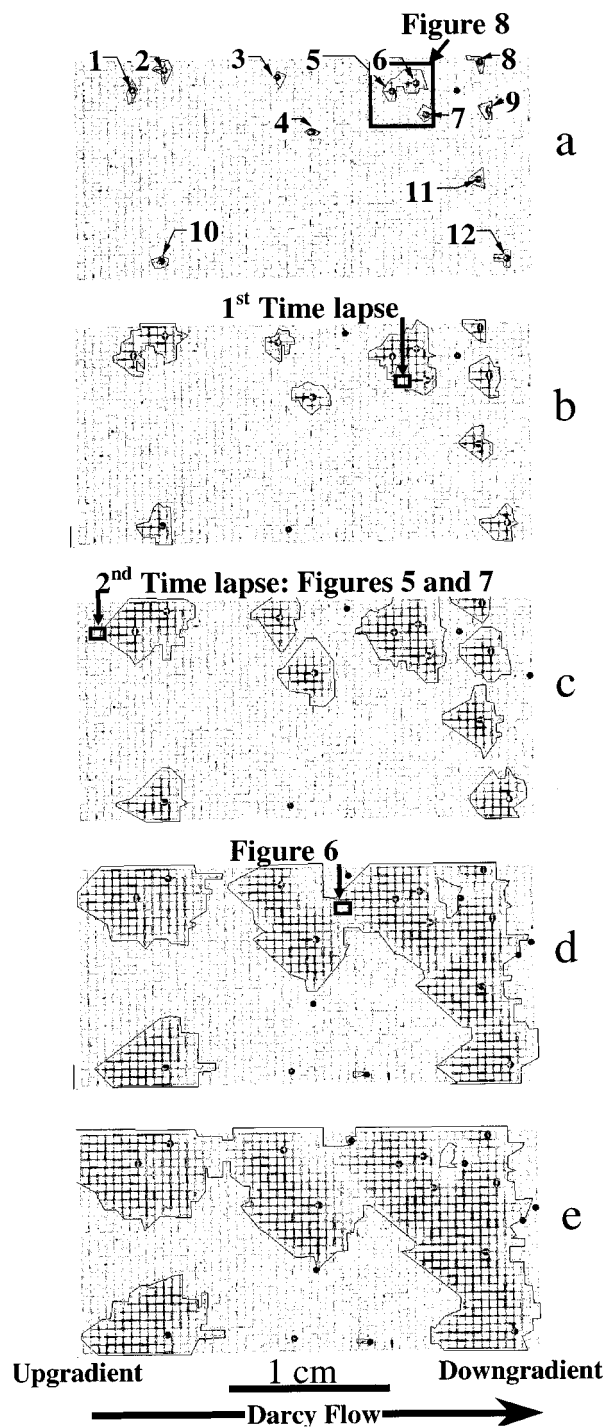


FIGURE 4. Meso-images of biological growth in the 13.5 mm by 28 mm SPIE at different times: (a) 1.94, (b) 2.52, (c) 2.95, (d) 3.62, and (e) 4.09 days. Numbered dots indicate position of initial expanding colonies. Unlabeled dots indicate position of later forming colonies. Lines represent colony boundaries as observed from microscopic images.

yielding an average intergrain velocity of 2.4 m/day. The temperature around the SPIE was 28 °C due to heating by the UV lamp.

Results

This paper describes growth that occurred during the first 4 days after feeding was started. Biological growth resulting within 1.35 days produced 12 colonies (Figure 4 a). Growth structure appeared similar for each colony. Each grew

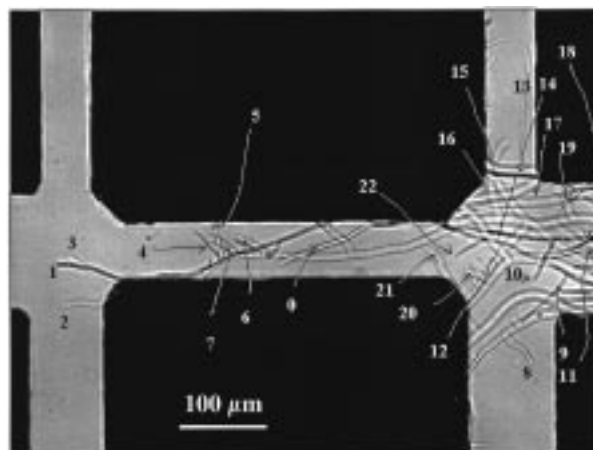


FIGURE 5. Filaments tracked to compute growth rates from time-lapse observations (Figure 4c).

producing long filaments about $6.5 \pm 2.3 \mu\text{m}$ wide, with lengths up to a few millimeters and with branching. Thinner filaments corresponded with younger sprouts. Collection and culturing of effluent spores at the end of the experiment suggested fungal growth dominated in the SPIE. This appeared similar to *Acremonium* sp. (personal communication with L. M. Ciuffetti). No other dominant microorganism was observed in the SPIE.

The pH of the effluent was between 2.6 and 3.3, while that of the feed was 6.6. The low effluent pH was probably due to nitric acid residues left in the dead volumes and perhaps caused the selection for fungal growth.

Mesoscale Observations. From the 12 initial starting colonies, a clear progression of filamentous growth resulted in expanding arrow shapes in an upgradient direction toward the nutrient supply as well as in lateral directions across the regional flow (Figure 4), with the rate of growth being about the same from colony to colony. The slope of each arrow side has an average of ± 1.32 , with a standard deviation of 0.12, based upon meso-images from colonies 1, 4, 10, and 11 at times 2.64, 2.95, 3.17, and 3.45 days (not all of which are shown). At the mesoscale (Figure 4a,d), colonies 1, 4, 10, 11, and 12 moved horizontally in the upgradient direction at an average rate of $1.5 \mu\text{m}/\text{min}$. These colonies appeared less affected by growth of upgradient colonies, although the above slope of the other colonies were quite similar. The slope of the expanding arrow represents also the ratio of the rate of the upgradient growth to the rate of growth in the lateral directions, which would be about $1.1 \mu\text{m}/\text{min}$. Local heterogeneity due to the variation in sizes of the channels did not seem to perturb this pattern; indeed such variations were probably averaged at the mesoscale shown.

Colonies also grew downgradient but in a less dense fashion. While it was difficult to count in each channel the dense individual filaments that grew in the upgradient direction (Figure 5), only a few filaments grew per channel downgradient. However, downgradient colonies grew initially similar to upgradient colonies (Figure 4c), suggesting that nutrients were then readily available downgradient of the upgradient colonies.

As the upgradient filaments grew denser, growth of downgradient filaments slowed. For example, the growth of colony 8 slowed after 2.52 days, while surrounding colonies 6, 7, and 9 bloomed (Figure 4). This suggests that the upgradient colonies blocked the substrate supply by clogging, scavenging the substrate, or synthesizing toxic byproducts, any of which might limit downgradient growth.

Microscale Observations. Sprouting of the 12 dominant colonies was observed by 1.35 days. Sprouting of eight new colonies occurred between 1.94 and 3.33 days. However, these

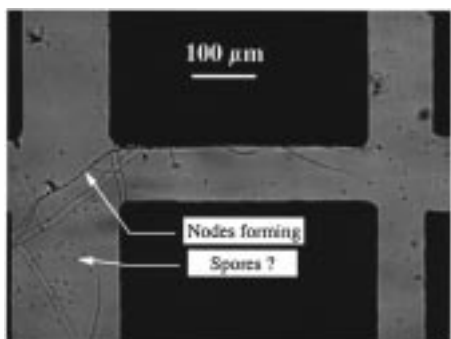


FIGURE 6. Illustration of nodes forming at $t = 3.89$ days.

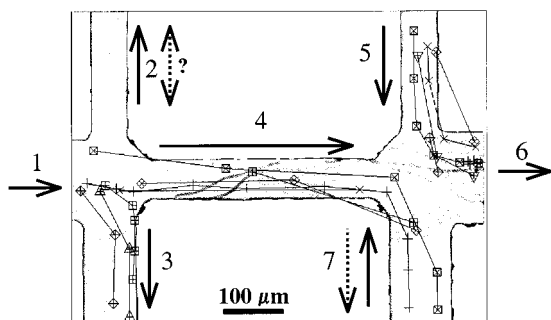


FIGURE 7. Observation of particles flowing in the network. Each observed particle has a different marker. Solid arrows indicate computed flow directions without growth. Dashed arrow indicates observed flow direction when different from computed one. The image was taken 105 min before that in Figure 5.

colonies did not extend beyond one or two channels. Observations of individual microimages indicated that no detachment of colonies occurred.

Frequent formation of nodes on filaments was observed (Figure 6) that subsequently disappeared from the filaments, suggesting they were spores. On other occasions, budding of a new filament would occur from the nodes. Filaments grew from their ends. Growth did not occur along the entire length as bends in filaments did not move, or at least they did not move in well identifiable patterns, that might suggest internal growth.

Rapid time-lapse measurements were made at two upgradient colony leading edge locations to observe the growth process. One was made beginning at $t = 2.42$ days with 1 min intervals and the other at 30 s intervals beginning at $t = 3.01$ days (Figure 5). From these time-lapse observations, we measured the growth rates of 28 filaments. These growth rates ranged almost uniformly between 0.45 and 1.59 $\mu\text{m}/\text{min}$ with one outlier at 2.16 $\mu\text{m}/\text{min}$. There was little obvious correlation between growth rate and location within the channels. Lowest values ($0.74 \pm 0.22 \mu\text{m}/\text{min}$) were associated with nine filaments shorter than 60 μm , which appeared to be bending to orient themselves toward the flow. Highest values ($1.34 \pm 0.28 \mu\text{m}/\text{min}$) were associated with 19 filaments longer than 60 μm . These measured growth rates are consistent with mesoscale colony expansion rates of 1.5 $\mu\text{m}/\text{min}$ in the upgradient direction and 1.1 $\mu\text{m}/\text{min}$ in the lateral direction.

Observation of naturally occurring moving particles (Figure 7) indicated flow directions. The flow from channel 1 split, the lower portion moving down into channel 3 and the upper portion into channel 4. Channel 4 flow appeared to move primarily into channel 7 while that from channel 5 moved into channel 6. At the junction of channels 5 and 6, a particle was observed circling through five images (2.5 min). Thus, a viscous eddy appeared to result, a phenomena

numerically simulated to occur in sinusoidal shaped pores (25). No particle was observed in channel 2. However, the path of the upper most particle at the junction of channels 1 and 2 indicates little if any flow occurred in channel 2. A separation of laminar flow from channel 1 between channels 3 and 4 is evident. Simulated flow for a clean SPIE indicated that flow directions based upon particle movement were reversed from the computed directions in channels 7 and perhaps in channel 2 as well. This suggests that the presence of filaments in the channels did modify the conductivity and therefore the flow path as would be expected. The location of growth (Figure 4c) makes flow reversal at the locations noted appear reasonable.

Discussion

The usefulness of a SPIE system for temporal observations of biological growth in porous media was demonstrated for one experiment in which filamentous growth dominated. Further experiments with other pore structures and with well-defined organisms having different colonization, and growth patterns should further aid in evaluation of biological growth in porous media and its effect on clogging. The SPIE system should be useful to study the effect of disinfection on clogging, the attachment properties of microorganisms, and the effect of advection and diffusion on microenvironment variations. Thus, SPIE observations should help in developing realistic simulation models for biological growth and clogging.

Transposition of observed processes from such two-dimensional network systems to three-dimensional media is possible. Indeed, such transposition is the purpose of similar flat plate simulators used, for example, in petroleum engineering. However, such transposition must be done with care. For example, because a three-dimensional network is better connected than a two-dimensional one (i.e. there are more bypasses around a single clogged channel in 3D than in 2D), a given porosity reduction would likely lead to a lesser permeability reduction in 3D than in 2D. However, if a phenomenological model is developed and calibrated with 2D observations, its extrapolation to a 3D model should be relatively straightforward.

The filamentous growth that we observed is only one possible realization of growth in porous media. Generalizations to other growth patterns commonly observed (4, 21) cannot be made from this one observation, but some generalizations about filamentous clogging are possible. With the filamentous fungal growth here observed, the more numerous and closer to each other downgradient colonies became intermingled and eventually spanned across the entire SPIE. However, the lower middle portion of the SPIE, which had no initial colonies, remained open and devoid of visible growth throughout the entire experiment. Thus, at the mesoscale, with heterogeneous initial seeding, growth distribution could also become heterogeneous, even when channel structure itself was a priori homogeneous. The patchiness that resulted thus appeared more related to the initial location of the colonies rather than to physical characteristics of the system. From an engineering point of view, this suggests that open pockets as observed here could result with bioremediation even in homogeneous formations.

To evaluate the possible influence of flow direction on growth, a simple network flow model was devised. Assumptions used are that no biological growth is present, the flow driven by a fixed head is fully developed and laminar, and the channel widths, lengths, and depths are similar to that in the SPIE. The resulting channel velocities are illustrated in Figure 8a,b for a section of the SPIE around colonies 5, 6, and 7. The arrows indicate the direction of flow with their lengths proportional to average channel velocity. This illustrates that dense growth generally occurred in an upgradient direction even when filament density was low

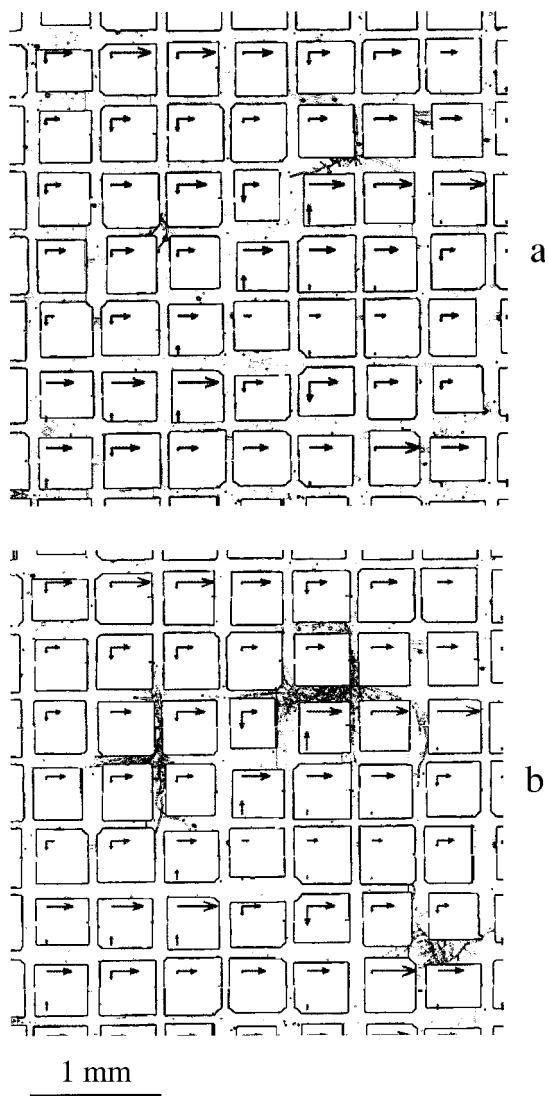


FIGURE 8. Simulation of the flow in the SPIE at $t = 0$, overlapped with a portion (Figure 4a) of the Sobel transform of the meso-image of the SPIE at different times: (a) 1.35 and (b) 1.94 days.

and nutrient concentration likely still high. New filaments from budding oriented themselves for upgradient growth. The marked direction and response of filament growth even at early times suggests that growth direction was sensitive to chemical gradients (chemotropism) and/or flow direction (rheotropism). However, because concentrations were not measured in situ, no definitive conclusion about such phenomena can be drawn. The measured upgradient filamentous growth rate of $1.5 \mu\text{m}/\text{min}$ is lower than the speed of many motile microorganisms, which if present might have enhanced colony spreading. This experiment did show that organized growth and colonization (due to chemotropism, rheotropism, byproducts toxicity, or other regulatory mechanism) can be important phenomena to address in modeling of bioclogging by filamentous organisms.

Downgradient filaments grew little and did not become dense like those in the upgradient direction. New colonies that appeared after 1.94 days remained small. This suggests that spore release and subsequent downgradient attachment would have little impact on biological growth, hence on clogging, in this system.

After a few days, growth became concentrated mainly in the upgradient portion of the colonies, and with time the

different colonies became more intermingled, with growth dominating only in the most upgradient end of the SPIE. This is consistent with observations that growth and clogging occur mainly around an injection well (2, 26). In this experiment, this occurred over a few millimeters.

Figure 4e shows a mesoscale image of a single irregular flow channel between two long intermingled colonies. Extensive growth occurred at the outer part of the colonies, while the inner parts grew minimally. Traditionally, biomass in porous medium is represented as growing at the surface of soil grains either as a biofilm (9, 16, 17) or microcolonies (19) or in more recent representations as packed clusters (11, 27) with advective flow between. In such cases, the thickness dimension of the biofilm is no larger than the micrometer or millimeter scale of the pore. However, with the filamentous growth measured here, a colony occupied many pores giving a much larger dimension approaching a centimeter in size.

Undoubtedly, this view of a mesoscale patchy biofilm separated by open flow channels at the mesoscale might also be expandable to the macroscale. If one connected this single mesoscale image with many other similar images in a three-dimensional view at a field scale or macroscale, a similar image is likely to result.

As a final remark, for in situ biological treatment of an aquifer where nutrients are supplied through a well for biological growth, this one experiment suggests clogging might be prevented if an operational method could be found to keep the channels open between biological colonies. More observations are needed to determine whether this is a general phenomena.

Acknowledgments

This research was supported in part by the Office of Research and Development, U.S. Environmental Protection Agency, through the Western Region Hazardous Substance Research Center under agreement R-815738, and in part by Elf Aquitaine, Inc. This article has not been reviewed by those organizations and thus no official endorsement should be inferred. Appreciation is extended to Lynda M. Ciuffetti, Oregon State University, for assistance in identifying the dominant organisms in the SPIE.

Literature Cited

- (1) Cunningham, A. B.; Characklis, W. G.; Abedeen, F.; Crawford, D. *Environ. Sci. Technol.* **1991**, *25*, 1305–1311.
- (2) Ehrlich, G. G.; Ku, H. F. H.; Vecchioli, J.; Ehlike, T. A. U.S. Geological Survey: Professional Paper 751-E, 1980.
- (3) Vecchioli, J.; Ku, H. F. H.; Sulam, D. J. U.S. Geological Survey: Professional Paper 751-F, 1980.
- (4) Vandevivere, P.; Baveye, P. *Soil Sci. Soc. Am. J.* **1992**, *56*, 1–13.
- (5) Taylor, S. W.; Milly, P. C. D.; Jaffe, P. R. *Wat. Resour. Res.* **1990**, *26*, 2161–2169.
- (6) Vandevivere, P.; Baveye, P. *Appl. Environ. Microbiol.* **1992**, *58*, 1690–1698.
- (7) Torbati, H. M.; Raiders, R. A.; Donaldson, E. C.; McInerney, M. J.; Jenneman, G. E.; Knapp, R. M. *J. Ind. Microbiol.* **1986**, *1*, 227–234.
- (8) Soares, M. I. M.; Belkin, S.; Abeliovich, A. *Z. Wasser Abwasser Forsch.* **1989**, *22*, 20–24.
- (9) Rittmann, B. E. *Water Resour. Res.* **1993**, *29*, 2195–2198.
- (10) Lewandowski, Z.; Altobelli, S. A.; Majors, P. D.; Fukushima, E. *Water Sci. Technol.* **1992**, *26*, 577–584.
- (11) Stoodley, P.; Debeer, D.; Lewandowski, Z. *Appl. Environ. Microbiol.* **1994**, *60*, 2711–2716.
- (12) Korber, D. R.; Lawrence, J. R.; Sutton, B.; Caldwell, D. E. *Microb. Ecol.* **1989**, *18*, 1–20.
- (13) Nivens, D. E.; Chambers, J. Q.; Anderson, T. R.; Tunlid, A.; Smit, J.; White, D. C. *J. Microbiol. Methods* **1993**, *17*, 199–213.
- (14) Cunningham, A. B.; Visser, E.; Lewandowski, Z.; Abrahamson, M. *Water Sci. Technol.* **1995**, *32*, 107–114.

- (15) Bishop, P. L.; Gibbs, J. T.; Cunningham, B. E. *Environ. Technol.* **1997**, *18*, 375–385.
- (16) Rittmann, B. E.; McCarty, P. L. *Am. Soc. Civil Engineers, J. Environ. Eng. Division* **1981**, *107*, 831–849.
- (17) Taylor, S. W.; Jaffe, P. R. *J. Environ. Eng. (ASCE) JOEEDU* **1991**, *117*, 25–46.
- (18) Suchomel, B. J.; Chen, B. M.; Allen, M. B., III *Transp. Porous Media* **1998**, *30*, 1–23.
- (19) Molz, F. J.; Widdowson, M. A.; Benefield, L. D. *Water Resour. Res. WRERAO* **1986**, *22*, 1207–1216.
- (20) Vandevivere, P.; Baveye, P.; Sanchez de Lozada, D.; DeLeo, P. *Water Resour. Res.* **1995**, *31*, 2173–2180.
- (21) Paulsen, J. E.; Oppen, E.; Bakke, R. *Water Sci. Technol.* **1997**, *36*, 1–9.
- (22) Laroche-Jaffrennou, C.; Vizika, O.; Kalaydjian, F. Wettability Heterogeneities in gas injection. Experiments and modelling. In *Proceedings of the 9th European Symposium on Improved Recovery*; The Hague, Netherlands, 1997.
- (23) Keller, A. A.; Blunt, M. J.; Roberts, P. V. *Transp. Porous Media* **1997**, *26*, 277–297.
- (24) Berkowitz, B.; Ewing, R. P. *Surv. Geophys.* **1998**, *19*, 23–72.
- (25) Dykaar, B. B.; Kitanidis, P. K. *Water Resour. Res.* **1996**, *32*, 307–320.
- (26) Taylor, S. W.; Jaffe, P. R. *Water Resour. Res.* **1990**, *26*, 2153–2159.
- (27) Lawrence, J. R.; Korber, D. R.; Hoyle, B. D.; Costerton, J. W.; Caldwell, D. E. *J. Bacteriol.* **1991**, *173*, 6558–6567.

Received for review November 6, 1998. Revised manuscript received February 4, 1999. Accepted February 4, 1999.

ES981146P